ACS Energy LETTERS

http://pubs.acs.org/journal/aelccp

ENERGY EXPRESS

Models of Oxygen Occupancy in Lead Phosphate Apatite $Pb_{10}(PO_4)_6O$

Kanta Ogawa, Kasper Tolborg, and Aron Walsh*

Cite This: *ACS Energy Lett.* 2023, 8, 3941−3944

Read Online

ACCESS | Metrics & More | Article Recommendations | Supporting Information

ABSTRACT: Lead phosphate apatite, the parent compound of the proposed room-temperature superconductor LK-99, features a $[Pb_{10}(PO_4)_6]^{II}$ scaffold with a charge-compensating oxide ion. This O^{-II} occupies a 4*e* site in the $P6_3/m$ unit cell, with 25% probability on average. We model the occupancy of this site from substoichiometric ($x = 0$) to superstoichiometric ($x = 4$) regimes in $Pb_{10}(PO_4)_6O_x$. Doping is predicted by adjusting the oxygen composition within the ⟨0001⟩ channel, with evidence for strong O−O correlation. This behavior introduces a sensitivity to the crystal growth and annealing conditions, with an opportunity for novel functionality to emerge.

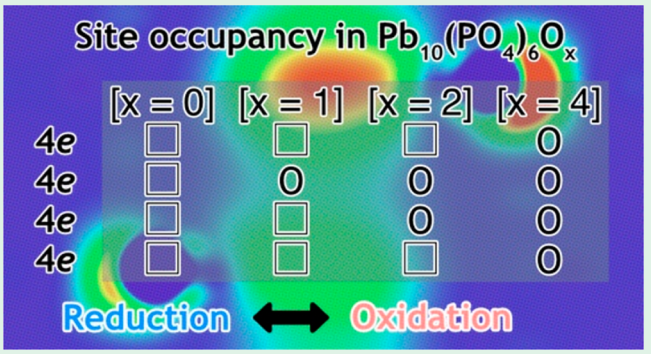

The Pb^{II} ion, with its characteristic Pb $6s^2$ lone electron pair, is a building block of materials widely used for energy conversion and storage. These include the family of lead halide perovskites used in photovoltaics, chalcogenide thermoelectrics, as well as oxide-based batteries and ferroelectric ceramics. In contrast, lead phosphates have drawn more attention in environmental chemistry,[1] until their recent study as hosts for room-temperature superconductivity when doped with Cu.[2,3] Ambient superconductivity has the potential to revolutionize energy transport and storage if realized in a reproducible and scalable form.

The stoichiometric combination of PbO and $NH_4H_2PO_4$ has been used to synthesize single crystals of $Pb_4(PO_4)_2O$, $Pb_8(PO_4)_2O_5$, and $Pb_{10}(PO_4)_6O$, where the formal 2+ charge of the Pb cation is balanced by phosphate (PO_4^{-III}) and oxide (O^{-II}) anions.[4] The latter compound crystallizes in an apatite-type crystal structure with the hexagonal space group $P6_3/m$. A key feature of the structure is two channels (Figure 1a). There are two distinct lead sites, with Pb(1) ions on 6*h* sites in channel 1 at $z = 1/4$ and 3/4, while the Pb(2) ions sit on 4*f* sites in channel 2 around $z = 0$ and 1/2. The structure obtained from refinement of single-crystal X-ray diffraction data features an oxide ion on a 4*e* site with 0.25 occupancy, on average.[4]

Here, we report an *ab initio* electronic structure and thermodynamic analysis of the $Pb_{10}(PO_4)_6O$ crystal in stoichiometric, oxidized, and reduced forms. We are motivated by both the chemical flexibility of the apatite structure and the known sensitivity of ceramic superconductors to oxide stoichiometry and strong O−O interactions.[5] One can envision conditions where the oxide sublattice is empty $Pb_{10}(PO_4)_6$, half-occupied $Pb_{10}(PO_4)_6O_2$, or filled $Pb_{10}(PO_4)_6O_4$. These oxidation and reduction reactions can be written as

$$Pb_{10}(PO_4)_6O \rightarrow Pb_{10}(PO_4)_6 + {}^1/_2O_2(g) \quad (1)$$

$$Pb_{10}(PO_4)_6O + {}^1/_2O_2(g) \rightarrow Pb_{10}(PO_4)_6O_2 \quad (2)$$

$$Pb_{10}(PO_4)_6O + {}^3/_2O_2(g) \rightarrow Pb_{10}(PO_4)_6O_4 \quad (3)$$

From the perspective of a defect process, the three reactions can be considered as the formation of an ordered defect compound of oxygen vacancies (eq 1) or oxygen interstitials (eqs 2 and 3). Total energy calculations of the reactants and products were performed using density functional theory with the PBEsol[6] exchange-correlation functional as implemented in VASP,[7] considering both scalar relativistic effects for structure relaxation and spin−orbit coupling (SOC) for the associated electronic structure and thermodynamic analysis, with a plane-wave basis set using a kinetic energy cutoff of 750 eV. The atomic forces were converged to within 0.01 eV/Å. We use a setup similar to the recent computational analysis of LK-99,[8] with full details reported in the Supporting Information (SI), section S1.

Received: August 9, 2023
Accepted: August 18, 2023
Published: August 28, 2023

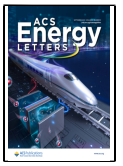

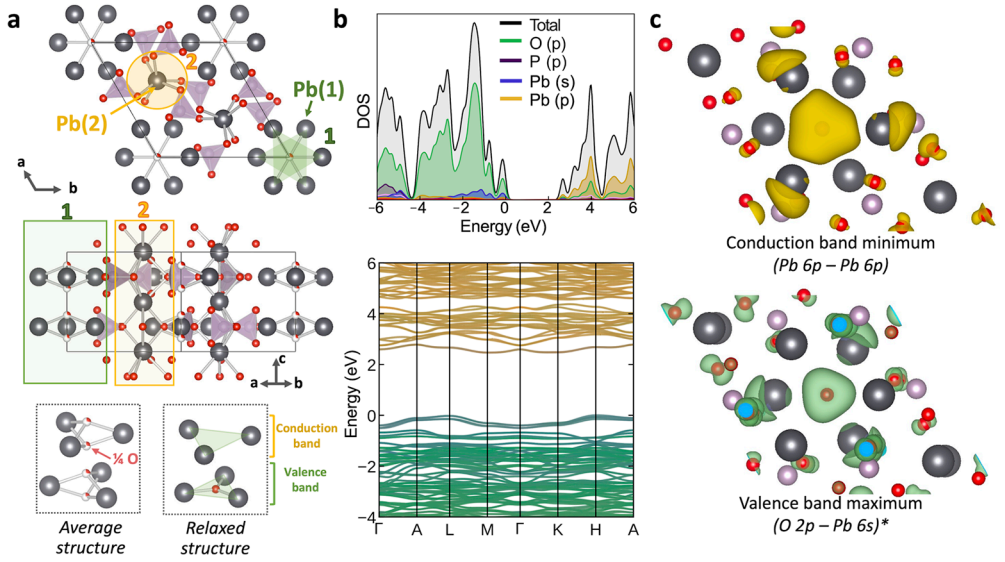

Figure 1. (a) Crystal structure of $Pb_{10}(PO_4)_6O$ highlighting the two ⟨0001⟩ channels and partially occupied oxide 4*e* site in channel 1. (b) Electron density of states and band structure (PBEsol+SOC), with features characteristic of Pb^{II} oxides.[9] The ⟨0001⟩ direction corresponds to the Γ-to-A line in reciprocal space. (c) Electron density map of the valence band maximum and conduction band minimum at an isosurface value of 0.0015 e/Å^3 around channel 1.

For stoichiometric $Pb_{10}(PO_4)_6O$, there is one configuration for the occupancy of the O 4*e* site in a single unit cell. Configurations involving supercell expansions are considered in Figure S1.

Structure optimization results in a large relaxation of the oxide coordinate along the *c* axis, from (0,0,0.134) to (0,0,0.242), where it moves to the same plane as Pb(1), Figure 1a. The valence and conduction bands are localized around channel 1, which contains the O 4*e* sites. Further chemical bonding analysis is provided in SI section S3 (Figures S2–S6). The electronic band dispersion in reciprocal space is anisotropic, with calculated electron (hole) effective masses of 1.5 (0.9) $m_e^{\perp}$ and 10.3 (3.7) $m_e^{\parallel}$, respectively (Table S1). Similarly, the high (low) frequency dielectric constants are calculated to be 4.4 (21.8) and 4.2 (48.6), respectively, within density functional perturbation theory.

Oxide loss (eq 1) leaves all 4*e* sites empty and results in a two-electron reduction. These excess electrons fill channel 1 due to the occupation of the conduction band formed of overlapping Pb 6p orbitals, Figure 2a, where SOC localizes two electrons in a Pb triangle. The localization of the electron density is characteristic of a low-dimensional electride.[10,11] These are the same 6p orbitals involved in forming the conduction band of Pb- and Bi-containing perovskites, where their overlap is determined by the topology of the crystal structure.[12]

For partial oxidation (eq 2), a second 4*e* site is occupied by O. This gives rise to three arrangements of O in a unit cell, i.e., [□OO□], [OO□□], and [□O□O], where □ represents an empty 4*e* site. We find evidence of strong O–O attraction, with relative energies of 0, 0.3, and 1.3 eV, respectively, for the three configurations further explored in Figure S9. Spontaneous peroxide formation quenches the generation of holes; i.e., two oxides interact to produce a peroxide anion (O_2^{-II}) with an O–O separation of 1.47 Å in the lowest energy nearest-neighbor configuration. We note that peroxide-doped apatite crystals are known.[13] Attempts to trigger a Pb bipolaron through manual distortions, i.e., alternative charge compensation by Pb(II) to Pb(IV) oxidation, proved unsuccessful.

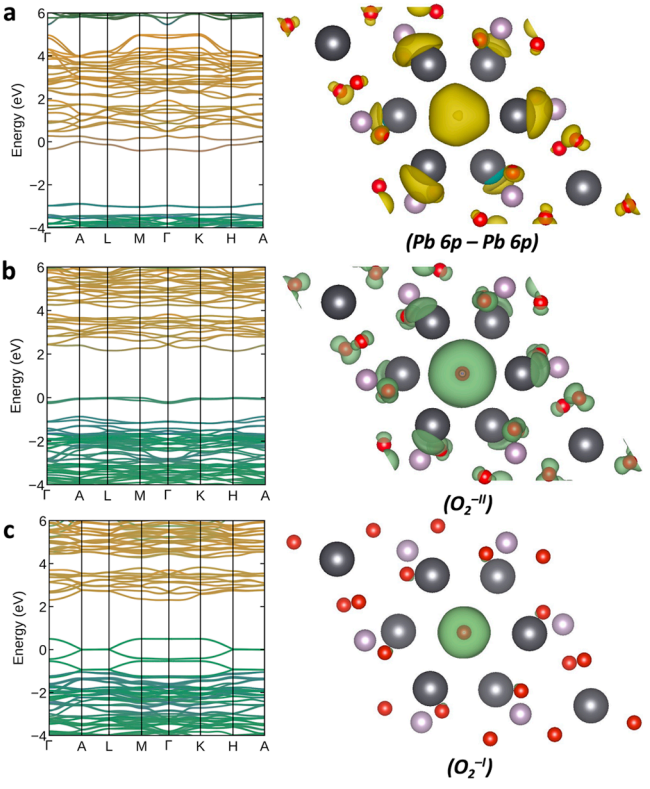

Figure 2. Electronic band structure and Fermi-level electron density of (a) *x* = 0 (electron-excess), (b) *x* = 2 (peroxide formation), and (c) *x* = 4 (superoxide formation) forms of $Pb_{10}(PO_4)_6O_x$ at an isosurface value of 0.0015 e/Å^3. Additional electronic analysis is provided in SI sections S4 (Figures S7 and S8), S6 (Figures S10–S13), and S7 (Figures S14 and S15).

For full oxidation (eq 3), all 4*e* sites are occupied by O. Here we again observe spontaneous dimerization, this time indicative of superoxide formation with the transition from

https://doi.org/10.1021/acsenergylett.3c01651
ACS Energy Lett. 2023, 8, 3941–3944

$4O^{-II}$ to $2O_2^{-I}$. A sequence of alternating long (2.29 Å) and short (1.36 Å) O−O connections emerges along the *c* axis. This process avoids oxidation and the generation of delocalized holes. The π_g^* orbitals in these two superoxide anions (O_2^{-I}) interact within the channel to produce a zero gap state (Figures 2c and S15). Again, superoxide anions have been reported in apatite channels.[13]

The calculated reaction thermodynamics are summarized in Table 1. Exchange with gaseous oxygen introduces a dependence on the chemical potential. We consider typical growth and ambient conditions of T = 1223 and 298 K, with representative low (1×10^{-6} atm) and high (1 atm) partial pressure of an O_2 ideal gas for reduction (eq 1) and oxidation (eqs 2 and 3), respectively. The formalism is further described in SI section S1. Oxygen loss and gain can proceed with relatively low energetic cost (<2 eV per oxygen exchange). None of the reactions are spontaneous, indicating that complete oxidation or reduction of $Pb_{10}(PO_4)_6O$ will not occur under typical processing conditions. While non-stoichiometry through partial occupancy of the 4*e* site under ultra-high-vacuum conditions can support a modest density of excess electrons ($K_{eq}^{(1)} = 2 \times 10^{-7}$), we predict that an appreciable concentration of peroxide anions will form with an equilibrium constant of $K_{eq}^{(2)} = 4 \times 10^{-4}$ for reaction 2 at high $p(O_2)$ and room temperature.

Table 1. Thermodynamics of Oxidation and Reduction[a]

Reaction	ΔG_{low} (eV), at T = 1223 K (298 K)	ΔG_{high} (eV), at T = 1223 K (298 K)
(1)	1.64 (3.31)	2.37 (3.48)
(2)	1.49 (0.38)	1.32 (0.20)
(3)	5.49 (2.15)	4.96 (1.62)

[a]The optimized cell parameters are a = 9.84 Å, c = 7.36 Å ($Pb_{10}(PO_4)_6O$); a = 9.80 Å, c = 7.28 Å ($Pb_{10}(PO_4)_6$); a = 9.71 Å, c = 7.34 Å ($Pb_{10}(PO_4)_6O_2$); and a = 10.03 Å, c = 7.29 Å ($Pb_{10}(PO_4)_6O_4$). The reaction energies are calculated for low (1×10^{-6} atm) and high (1 atm) $p(O_2)$ from the sum of products minus the sum of reactants.

In summary, the underlying electronic structure of $Pb_{10}(PO_4)_6O$ is typical of Pb^{II} heteropolar crystals used in optoelectronic and energy conversion technologies, with strong features of the Pb $6s^2$ lone pair. Such chemical features have been highlighted for the Cu-doped compound[8] and in the context of $Ba(Bi,Pb)O_3$ superconductors.[14] We noted a deviation in the relaxed O 4*e* coordinate from the original experimental structure, while a recent reinvestigation of the crystal structure has also highlighted the complexity of oxygen ordering.[15] It has also been suggested that the synthesis route for LK-99 can lead to hydroxide formation, i.e., $Pb_{10}(PO_4)_6(OH)_2$,[15,16] with the possibility of the channel being occupied by various combinations of O, O_2, OH, and site vacancies, depending on the material processing conditions.

There are signs of an intrinsic resistance to hole doping in lead phosphate apatite, with spontaneous peroxide and superoxide formation bridging the O sites and avoiding free charge carrier generation. The oxygen content in the channel significantly affects the local electronic structure of the material from a large gap insulator to a small or a zero gap state. The mobility of oxygen in this channel, the inclusion of hydrogen and hydroxide, and the influence of oxygen stoichiometric variations on extrinsic impurities such Cu will make this a fertile crystal system for further investigation of defect processes in low dimensions.

■ ASSOCIATED CONTENT

Supporting Information

The Supporting Information is available free of charge at https://pubs.acs.org/doi/10.1021/acsenergylett.3c01651.

Electronic structure and chemical bonding analysis (PDF)

Accession Codes

The input and output files involved in this study have been uploaded to the NOMAD repository at 10.17172/NOMAD/2023.08.10-1.

■ AUTHOR INFORMATION

Corresponding Author

Aron Walsh − *Department of Materials, Imperial College London, London SW7 2AZ, U.K.; Department of Physics, Ewha Womans University, Seoul 03760, Korea;* orcid.org/0000-0001-5460-7033; Email: a.walsh@imperial.ac.uk

Authors

Kanta Ogawa − *Department of Materials, Imperial College London, London SW7 2AZ, U.K.*

Kasper Tolborg − *Department of Materials, Imperial College London, London SW7 2AZ, U.K.;* orcid.org/0000-0002-0278-115X

Complete contact information is available at: https://pubs.acs.org/10.1021/acsenergylett.3c01651

Notes

The authors declare no competing financial interest.

■ ACKNOWLEDGMENTS

This work was supported by the JSPS overseas program, and the Eric and Wendy Schmidt AI in Science Postdoctoral Fellowship, a Schmidt Futures program. Via the authors' membership of the UK's HEC Materials Chemistry Consortium, which is funded by EPSRC (EP/X035859/1), this work used the ARCHER2 UK National Supercomputing Service (http://www.archer2.ac.uk).

■ REFERENCES

(1) Santillan-Medrano, J.; Jurinak, J. J. The Chemistry of Lead and Cadmium in Soil: Solid Phase Formation. *Soil Sci. Soc. Am. J.* **1975**, *39* (5), 851−856.

(2) Lee, S.; Kim, J.-H.; Kwon, Y.-W. The First Room-Temperature Ambient-Pressure Superconductor. *arXiv Preprint* **2023**, DOI: 10.48550/arXiv.2307.12008.

(3) Lee, S.; Kim, J.; Im, S.; An, S.; Kwon, Y.-W.; Auh, K. H. Consideration for the development of room-temperature ambient-pressure superconductor (LK-99). *J. Korean Cryst. Growth Cryst. Technol.* **2023**, *33* (2), 61−70.

(4) Krivovichev, S. V.; Burns, P. C. Crystal Chemistry of Lead Oxide Phosphates: Crystal Structures of $Pb_4O(PO_4)_2$, $Pb_8O_5(PO_4)_2$ and $Pb_{10}(PO_4)_6O$. *Z. Krist. - Cryst. Mater.* **2003**, *218* (5), 357−365.

(5) Stoneham, A. M.; Smith, L. W. Defect Phenomena in Superconducting Oxides and Analogous Ceramic Oxides. *J. Phys.: Condens. Matter* **1991**, *3* (3), 225−278.

(6) Perdew, J. P.; Ruzsinszky, A.; Csonka, G. I.; Vydrov, O. A.; Scuseria, G. E.; Constantin, L. A.; Zhou, X.; Burke, K. Restoring the

Density-Gradient Expansion for Exchange in Solids and Surfaces. *Phys. Rev. Lett.* **2008**, *100* (13), 136406.
(7) Kresse, G.; Furthmüller, J. Efficient Iterative Schemes for Ab Initio Total-Energy Calculations Using a Plane-Wave Basis Set. *Phys. Rev. B* **1996**, *54* (16), 11169.
(8) Griffin, S. M. Origin of Correlated Isolated Flat Bands in Copper-Substituted Lead Phosphate Apatite. *arXiv Preprint* **2023**, DOI: 10.48550/arXiv.2307.16892.
(9) Walsh, A.; Payne, D. J.; Egdell, R. G.; Watson, G. W. Stereochemistry of Post-Transition Metal Oxides: Revision of the Classical Lone Pair Model. *Chem. Soc. Rev.* **2011**, *40* (9), 4455−4463.
(10) Liu, C.; Nikolaev, S. A.; Ren, W.; Burton, L. A. Electrides: A Review. *J. Mater. Chem. C* **2020**, *8* (31), 10551−10567.
(11) Zhang, Y.; Xiao, Z.; Kamiya, T.; Hosono, H. Electron Confinement in Channel Spaces for One-Dimensional Electride. *J. Phys. Chem. Lett.* **2015**, *6* (24), 4966−4971.
(12) Ogawa, K.; Suzuki, H.; Walsh, A.; Abe, R. Orbital Engineering in Sillén−Aurivillius Phase Bismuth Oxyiodide Photocatalysts through Interlayer Interactions. *Chem. Mater.* **2023**, *35* (14), 5532−5540.
(13) Ptáček, P. Substituents and Dopants in the Structure of Apatite. *Apatites and their Synthetic Analogues - Synthesis, Structure, Properties and Applications*; IntechOpen, 2016.
(14) Sleight, A. W. Chemistry of High-Temperature Superconductors. *Science* **1988**, *242* (4885), 1519−1527.
(15) Krivovichev, S. V. The Crystal Structure of $Pb_{10}(PO_4)_6O$ Revisited: The Evidence of Superstructure. *arXiv Preprint* **2023**, DOI: 10.48550/arXiv.2308.04915.
(16) Jiang, Y.; Lee, S. B.; Herzog-Arbeitman, J.; Yu, J.; Feng, X.; Hu, H.; Călugăru, D.; Brodale, P. S.; Gormley, E. L.; Vergniory, M. G.; Felser, C.; Blanco-Canosa, S.; Hendon, C. H.; Schoop, L. M.; Bernevig, B. A. $Pb_9Cu(PO_4)_6(OH)_2$: Phonon Bands, Localized Flat Band Magnetism, Models, and Chemical Analysis. *arXiv Preprint* **2023**, DOI: 10.48550/arXiv.2308.05143.

https://doi.org/10.1021/acsenergylett.3c01651
ACS Energy Lett. 2023, 8, 3941−3944